POAC'23
Glasgow, United Kingdom

Proceedings of the 27th International Conference on
Port and Ocean Engineering under Arctic Conditions
12-16 June 2023, Glasgow, United Kingdom

The effects of porosity on the flexural and uniaxial compressive strength of sea ice in the summer Arctic

Qingkai Wang[1], Zhijun Li[1], Bing Tan[2]
[1] State Key Laboratory of Coastal and Offshore Engineering, Dalian University of Technology, Dalian, China
[2] School of Mathematics and Statistics, Nanyang Normal University, Nanyang, China

ABSTRACT

Sea ice blocks were extracted in the summer Arctic during the Chinese National Arctic Research Expedition in 2021, which were then machined to small-scale samples for mechanical experiments. Three-point bending tests were performed at ice temperatures of −12 to −3ºC for columnar ice; and uniaxial compressive tests were performed at ice temperatures of −8 to −3ºC and strain rates of 10^{-6} to 10^{-2} s^{-1} for both columnar and granular ice. The ice density and salinity of ice samples were measured to determine brine and gas volume fractions. Results showed that sea ice flexural strength decreased with increasing porosity, and a mathematical equation was established to fit the trend. Sea ice flexural strength is independent of brine volume. The sea ice strain modulus was also independent on brine volume and porosity. Sea ice uniaxial compressive strength decreased with increasing porosity at both ductile and brittle strain rate regimes. Three dimensional surfaces were obtained of the uniaxial compressive strength varying with strain rate and porosity, which showed the transition strain rates from ductile to brittle regimes decreased with increasing sea ice porosity.

KEY WORDS: Sea ice porosity; Flexural strength; Uniaxial compressive strength; Arctic.

INTRODUCTION

The mechanical properties of sea ice play important roles in the sea ice dynamic and engineering processes. In the recent years, the rate of Arctic warming was estimated to be faster than that previously reported (Rantanen et al., 2022), leading to an accelerated melting of sea ice and probably weakened strength. Consequently, the ice force exerted on the ship and offshore structure in the waters where ice is present would be reduced, which causes excessive and uneconomic outcomes applying the design codes using sea ice mechanical properties derived from measurements conducted decades ago.

It is generally accepted that sea ice mechanics is largely dependent on its physical properties.

The relationship between sea ice uniaxial compressive strength and porosity has been quantified in previous studies (Moslet, 2007; Timco and Frederking, 1990), whereas, the commonly used equations to calculate sea ice flexural strength are still based on sea ice brine volume fraction (Timco and O'Brien, 1994). For warm ice in the summer Arctic, the brine drainage and meltwater flushing cause a lower content of brine than gas (Wang et al., 2020), leading to an overestimated flexural strength using Timco and O'Brien's equation.

With the Arctic Ocean becoming more accessible in summer, marine activities have increased in this region, which leads to higher demand for structures purposely built for the summer window period. Therefore, understanding the mechanical properties of summer sea ice is urgent. On one hand, sea ice physical properties change with sea ice getting warmer during an annual cycle. On the other hand, in response to the global warming, even for summer melting sea ice, Wang et al. (2020) found that both density and salinity of sea ice in recent years decreased compared to decades ago. Therefore, more studies are essential to update our knowledge on the Arctic sea ice mechanical properties since these properties have probably changed, which could be insightful to the response of Arctic sea ice to global warming.

To investigate the mechanical properties of current summer Arctic sea ice and their dependences on sea ice porosity, ice blocks were collected in the Central Arctic Ocean during ice melt season, which were stored for subsequent experiments on sea ice physical and mechanical properties performed in the domestic laboratory. In this study, we present the mechanical experiment results of flexural strength, strain modulus, and uniaxial compressive strength of Arctic sea ice.

FIELD SAMPLING AND LABORATORY TESTS

Overview of field sampling

During the Chinese National Arctic Research Expedition in 2021, two ice blocks were lifted onto the deck using the ship crane at ice sites S1 (85.7° N, 86.2° E) and S2 (85.9° N, 87.9° E) in the Central Arctic Ocean on 9 August 2021 (UTC), when the RV Xuelong2 stopped in the pack ice zone. The detailed information of ice blocks is listed in Table 1. The ice temperature was −0.6°C at S1 site and −1.1°C at S2 site, indicating the ice was melting. Further visual check showed no cracks on the appearance of ice block, only the top of ice damaged partly due to interaction with ship hull. Immediately after visual check, the two ice blocks were archived carefully using plastic bags to avoid sublimation, and stored at a surrounding temperature of −20°C without solar radiation in a cold room. The ice blocks were finally shipped to a low temperature laboratory at home after a 2-month expedition for detailed studies of crystal texture and mechanical properties.

Table 1. The information of ice blocks

Ice site	Ice thickness (cm)	Snow thickness (cm)	Air temperature (°C)	Ice temperature (°C)	Crystal structure
S1	130	10.7	−0.1	−0.6	Top granular ice followed by columnar ice
S2	160	11.9	0.2	−1.1	

The crystal structures of ice blocks were measured by preparing thin sections and observing under crossed polarized light. Both ice blocks showed a granular ice layer at the top underlain

by columnar ice layer until the bottom, which is the typical texture structure of first-year ice. The granular ice was at the top 35 cm approximately at S1 site, and 40 cm approximately at S2 site. The granular ice was fine-grained with a size of 1–2 mm in diameter.

Laboratory tests

The large ice blocks were machined into regular specimens in the cold laboratory before they were tested. Two types of sea ice mechanical tests were performed including three-point bending test and uniaxial compressive strength test. For the three-point bending test, small ice beams with long axis horizontal to original ice surface were cut first from large blocks using chain saw, which were then processed carefully using band saw to make rectangular cross-section with dimensions of 7 × 7 cm. The long axis of the ice beam was finally cut to 55 cm using band saw. After preparation, the ice samples were saved in a thermotank at the temperatures to be tested (−12, −8, −5 and −3°C) for at least 24 h to achieve phase equilibrium, and thus the sea ice porosities were ensured to be changed. For the uniaxial compressive strength test, the rough-cut ice cuboids were prepared first out of large ice block using a chain saw, which were then machined with care to section dimensions of 7 × 7 cm and length of 17.5 cm using the band saw. The ice samples were finally stored in a thermotank at required temperatures for tests (−8, −5, −3°C) for at least 24 h.

A small universal testing machine was used to perform the sea ice bending tests (Fig. 1a). The loaded plate of the machine was fitted with a stainless-steel column to give a line force on the midspan of the ice beam, which was supported by a frame with a span of 50 cm between two supports. The device was equipped with a force sensor of 3 kN capacity and ±1 % accuracy to measure the force exerted on the beam midspan and a displacement sensor with ±1 % accuracy to measure the displacement of loaded plate. Both force and displacement were recorded at frequencies of 50 Hz. The loading time of bending test was less than 30 s, corresponding to a strain rate range of 10^{-5}–10^{-2} s^{-1}. The uniaxial compressive strength test was conducted using a large universal testing machine (Fig. 1b). The machine is equipped with a force sensor of 100 kN capacity and ±0.5 % accuracy as well as a displacement sensor with ±2 μm accuracy. Both force and displacement were recorded at frequencies of 50 Hz. The test strain rates were from 10^{-6} s^{-1} to 10^{-2} s^{-1}. The columnar ice samples were compressed in the directions vertical and horizontal to ice surface and the granular ice samples were compressed in the direction horizontal to ice surface.

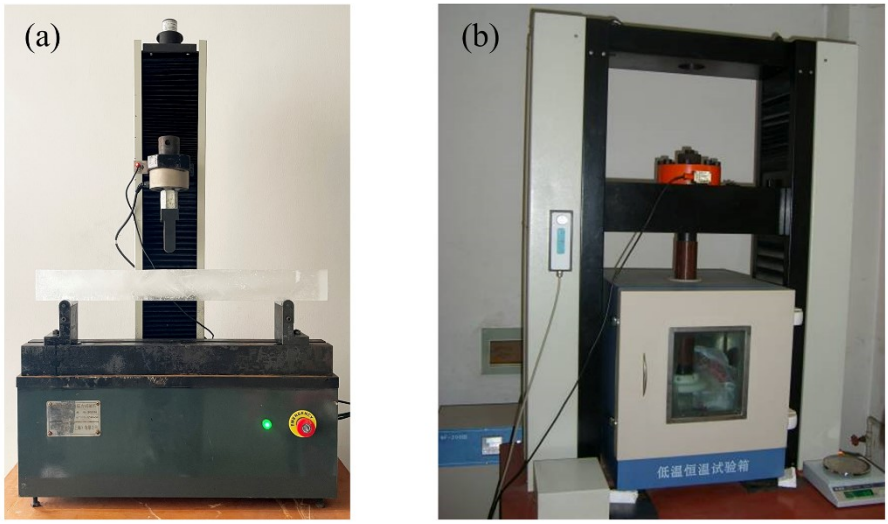

Figure 1. Test machine for sea ice three-point bending test (a) and uniaxial compressive strength test (b)

Before loading, the ice density was calculated using mass/volume method. After failure, the broken ice was collected to melt for salinity measurement using a salinometer. The brine and gas volume fractions as well as porosity of ice were then determined using sea ice temperature, salinity, and density according to Cox and Weeks (1983).

Thirty-eight ice beams with failure in the midspan were analyzed in this paper. The flexural strength and strain modulus were determined as Eq. (1) and (2):

$$\sigma_{\mathrm{f}} = \frac{3Fl}{2bh^2} \tag{1}$$

$$E = \frac{Fl^3}{4bh^3\delta} \tag{2}$$

where σ_{f} is ice flexural strength, E is strain modulus, F is load at ice failure, l is span between supports, b is sample width, h is sample height, and δ is the midspan deflection of beam.

A total of 156 ice samples were prepared for uniaxial compressive strength tests, of which 110 samples were columnar ice and 46 samples were granular ice. The sea ice uniaxial compressive strength was calculated as Eq. (3):

$$\sigma_{\mathrm{c}} = \frac{F_{\max}}{bd} \tag{3}$$

where σ_{c} is ice uniaxial compressive strength, $F_{\max}$ is maximum recorded force, and d is sample length.

RESULTS

Flexural strength

A total of 4 granular samples were tested in the bending tests under −3ºC with an average of

369 kPa and standard deviation of 72 kPa, which was lower than the flexural strength of columnar ice at the same test temperature (644 ± 195 kPa), because of higher porosity of granular ice (26.1 ± 6.3 %) than columnar ice (13.5 ± 4.5 %). Given the small amount of granular ice samples, only the flexural strength of columnar ice was analyzed below.

The porosity, brine volume fraction, and gas volume fraction of columnar ice samples were 5–20 %, 0.2–2.5 %, and 3.5–18.6 %, respectively. In the previous studies, the flexural strength of cold ice was related to the brine volume fraction (Karulina et al., 2019; Timco and O'Brien, 1994), and thus, the effect of brine volume on our ice strength was investigated first here. Since the brine volume fractions were small, to show the varying trend of flexural strength with brine volume fraction clearly, the fractions were expressed using square roots. To further reduce the effect of inherent scatter of sea ice mechanical tests, mean strength and standard deviation were determined taking the square root of brine volume fraction using bins of 0.02 width. The relationship between sea ice flexural strength and square root of brine volume fraction is depicted in Fig. 2a. Regression analysis using commonly used functions (e.g., linear, power, logarithmic, and exponential functions) were adopted to investigate the relationships between flexural strength and square root of brine volume fraction. However, even the highest determination coefficient (R^2) for power equation was still less than 0.2, and it was also not significant at a significance level (p) of 0.1.

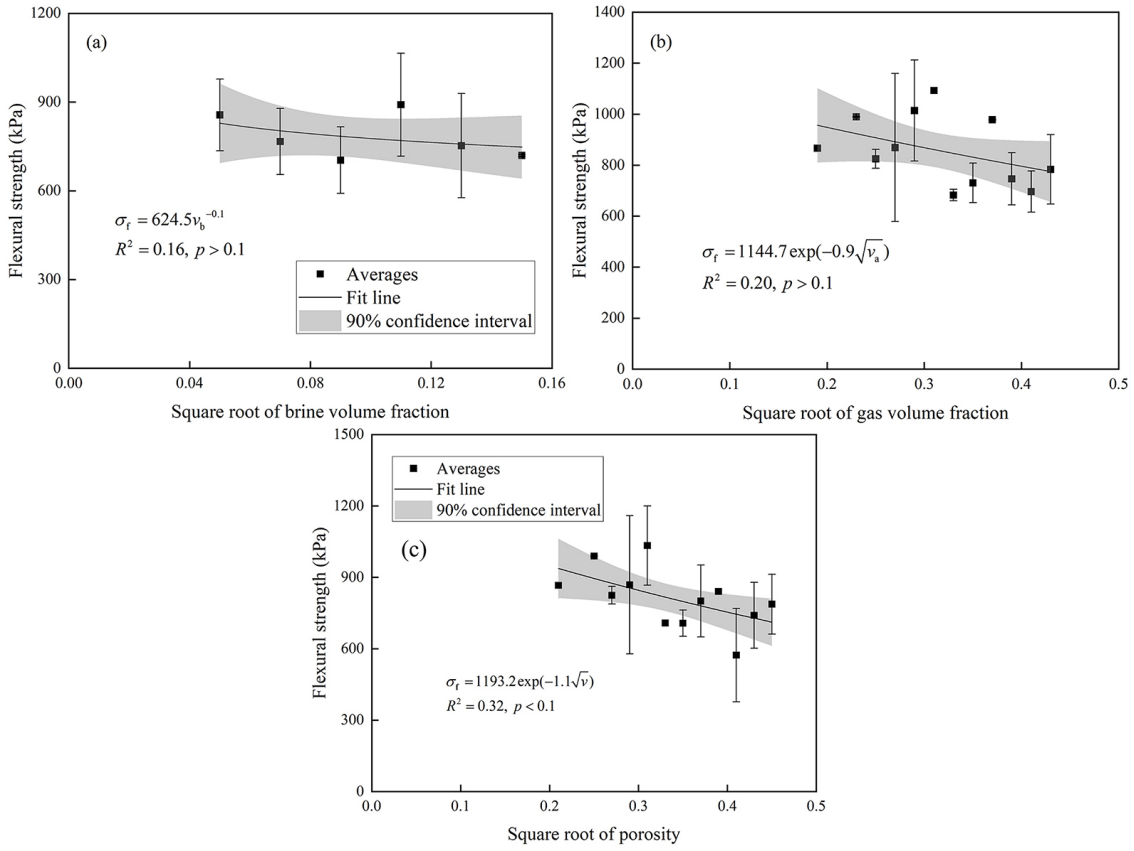

Figure 2. The variations of sea ice flexural strength with square root of (a) brine vol ume fraction, (b) gas volume fraction, and (c) porosity

It is noteworthy that the gas occupied much more space in ice samples than brine. Therefore, the effect of gas on the sea ice flexural strength cannot be neglected. For a better comparison with brine volume fraction, using the similar processing method as brine, the mean flexural strength and standard deviation were determined taking the square root of gas volume

fraction of 0.02 as a bin. The varying trend of sea ice flexural strength with square root of gas volume fraction is shown in Fig. 2b. The exponential function was the best regression form to depict the varying trend, but the relationship was also weak only with R^2 = 0.20 and not significant at p = 0.1 level.

Sea ice porosity is the sum of brine and gas volume fractions, and the dependence of sea ice flexural strength on porosity was then checked. The mean strength and standard deviation were determined taking the square root of porosity of 0.02 as a bin, and the relationship between sea ice flexural strength and square root of porosity is depicted in Fig. 2c. Sea ice flexural strength decreased with increasing porosity. Regression analysis found that the exponential form (Eq. 4) performed best with higher R^2 = 0.32 out of other commonly used functions including linear, logarithmic, and power functions, which was significant at p = 0.1 level.

$$\sigma_f = 1193.2 \exp(-1.1\sqrt{v}) \quad (5\% < v < 20\%) \tag{4}$$

where v is sea ice porosity.

Strain modulus

The strain modulus of granular ice was 1.6–6.7 GPa with an average of 3.2 ± 2.3 GPa, which was similar to that of columnar ice of 1.6–8.4 GPa with an average of 3.1 ± 1.2 GPa. Considering the limited amount of granular ice samples, the strain modulus of granular ice was still excluded in the analysis below.

Using the similar processes as flexural strength, the strain modulus was averaged taking 0.02 of square root of porosity, brine volume fractions, and gas volume fraction as bins, respectively, to examine the dependences of sea ice strain modulus on the ice phase composition. The relationship between sea ice strain modulus and porosity is shown in Fig. 3a. Regression analysis gave the linear equation as the best fit form out of commonly used mathematical expressions, but the relationship was weak only with R^2 = 0.15 and not significant at p = 0.1 level, indicating that sea ice strain modulus was not dependent on sea ice porosity.

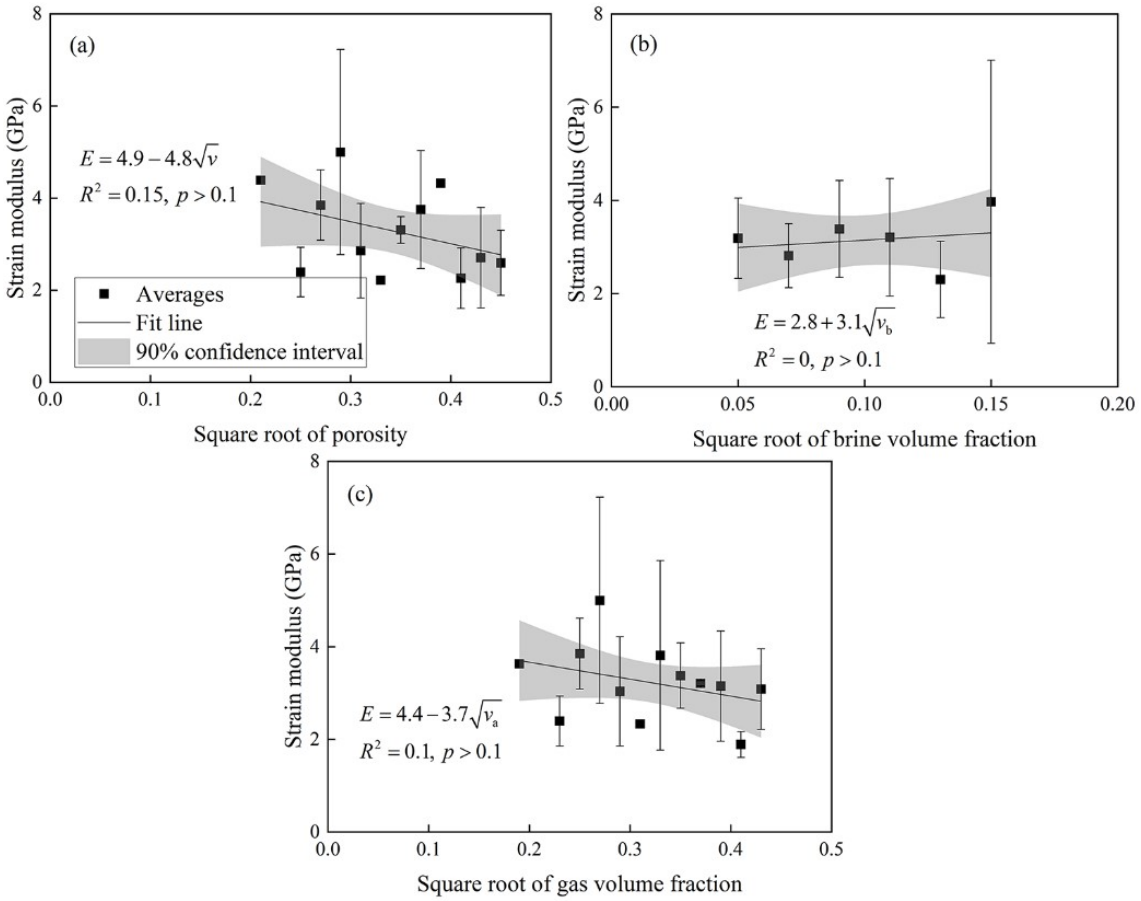

Figure 3. The variations of sea ice strain modulus with square root of (a) porosity, (b) brine volume fraction, and (c) gas volume fraction

The varying trends of sea ice strain modulus with brine and gas volume fractions are given in Figs. 3b and 3c. The best fit equations to depict the dependences of sea ice strain modulus on brine and gas volume fractions were identified, but the relationships between strain modulus and brine as well as gas volume fractions were quite weak with $R^2 < 0.1$ (even approaching 0 for brine volume fraction) and not significant at $p = 0.1$ level.

Uniaxial compressive strength

The brine and gas volume fractions were separated first to check their respective influences on uniaxial compressive strength. The brine and gas volume fractions of compressive samples were 0–3.8 % and 1.8–36.9 %, respectively. Using similar processes as analyzing flexural strength, the uniaxial compressive strength of vertically loaded columnar samples, horizontally loaded columnar samples, and granular samples were averaged taking the square root of brine and gas volume fractions of 0.02 as a bin. Regression analysis showed that there were no significant dependences of uniaxial compressive on brine and gas volume fractions ($R^2 < 0.2$ and $p > 0.1$).

It is generally accepted that sea ice porosity is the primary factor affecting sea ice uniaxial compressive strength. The sea ice porosity was 3.3–24.7 %, 9.0–21.9 %, and 9.8–36.9 % for

vertically loaded columnar samples, horizontally loaded columnar samples, and granular samples, respectively. Figure 4 shows the variations of uniaxial compressive strength with sea ice porosity, in which the mean strength and standard deviation were determined taking 0.05 of porosity as a bin. The uniaxial compressive strength decreased with increasing porosity, and further regression analysis showed that the varying trends could be described using the power law for all three types of tests with $R^2 > 0.8$ and at $p < 0.1$ level at least.

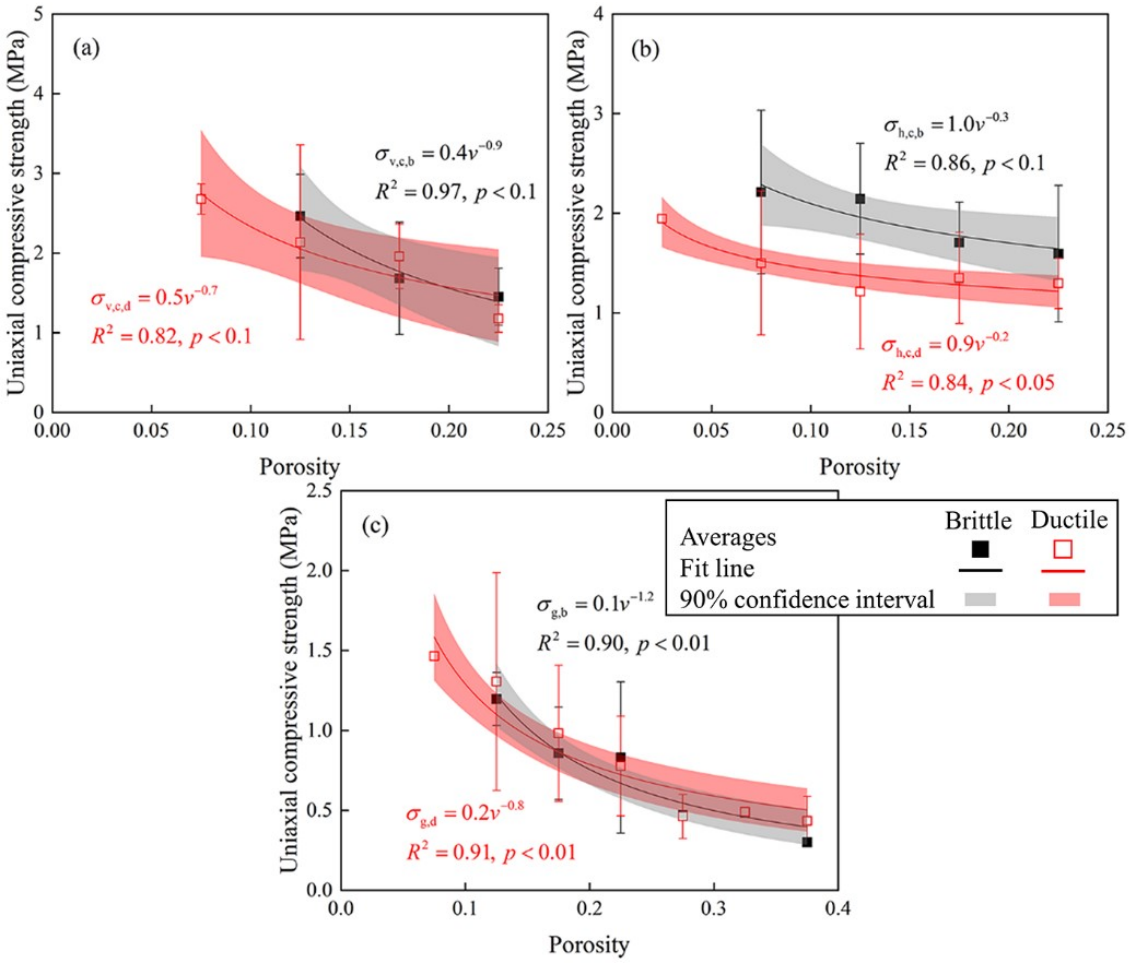

Figure 4. The variations of sea ice uniaxial compressive strength with porosity for (a) vertically loaded columnar samples, (b) horizontally loaded columnar samples, and (c) granular samples. The subscripts v, h, c, g, b and d represent vertical loading, horiz ontal loading, columnar ice, granular ice, brittle regime, and ductile regime, respective ly

It was noteworthy that the effect of strain rate on the uniaxial compressive strength was not separated in the Fig. 4. Ductile failure occurred at low strain rates, and brittl e failure occurred at high strain rates. The uniaxial compressive strength shows rate-st rengthening at ductile strain rate regime and rate-weakening at brittle strain rate regim e (Wang et al., 2022). Consequently, both sea ice porosity and strain rate were requir ed to describe the variations of sea ice uniaxial compressive strength in ductile and b rittle regimes. The three-dimensional surfaces shown in Fig. 5 exhibited the varying tr ends of uniaxial compressive strength, in which Eq. (5) was adopted using two-param

eter regression analysis, given the respective mathematical forms of uniaxial compressi ve strength with porosity and strain rate.

$$\sigma_c = A\dot{\varepsilon}^B v^C \tag{5}$$

where $\dot{\varepsilon}$ is strain rate, and A, B, and C are fitting coefficients listed in Table 2.

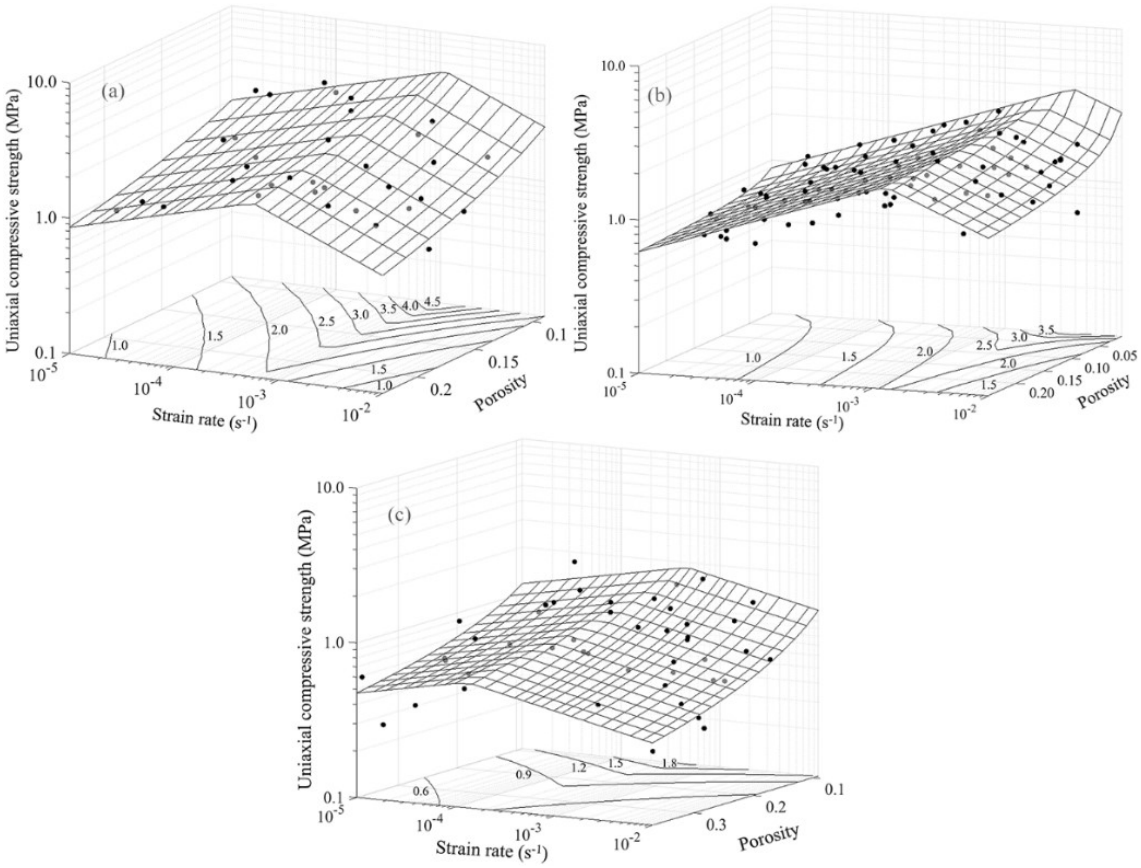

Figure 5. Three-dimensional surfaces of sea ice uniaxial compressive strength varying with porosity and strain rate for (a) vertically loaded columnar samples, (b) horizontal ly loaded columnar samples, and (c) granular samples

Table 2. The fitting coefficients of Eq. (5). The superscripts α and β represent significance levels of 0.01 and 0.05, respectively.

Sample	Ductile regime				Brittle regime			
	A	B	C	R^2	A	B	C	R^2
Vertically loaded columnar	2.27	0.20	−0.91	0.51^{α}	0.02	−0.33	−1.29	0.74^{α}
Horizontally loaded columnar	9.18	0.25	−0.11	0.60^{α}	0.15	−0.33	−0.31	0.43^{α}
Granular	1.02	0.12	−0.63	0.48^{α}	0.07	−0.15	−0.88	0.42^{β}

The uniaxial compressive strength reaches peak when sea ice transits from ductile to brittle behaviors. It was found from Fig. 5 that there were different ductile-to-brittle strain rates at

different porosities. The transition strain rates were 4.0×10^{-4}–1.0×10^{-3} s^{-1} for vertically loaded columnar samples, 1.0×10^{-3}–3.0×10^{-3} s^{-1} for horizontally loaded columnar samples, and 1.0×10^{-4}–4.0×10^{-4} s^{-1} for granular samples. Moreover, the transition strain rate decreased with increasing sea ice porosity. The transition from ductile to brittle behavior of sea ice can be regarded as a competition between stress relaxation and stress build-up (Schulson, 2001). The stress build-up occurs at crack tips. Brine inclusions and gas bubbles in sea ice work as pre-cracks facilitating stress concentration at crack tip. Therefore, with sea ice porosity increasing, stress concentration can be triggered at a lower strain rate.

CONCLUSIONS

Arctic sea ice blocks were taken during the Chinese National Arctic Research Expedition in 2021 summer for mechanical experiments. Three-point bending tests and uniaxial compressive strength tests were carried out to measure the sea ice flexural strength, strain modulus, and uniaxial compressive strength. The porosity of each ice sample was determined according to the measurements of ice temperature, salinity, and density. Both flexural strength and uniaxial compressive strength of summer Arctic sea ice were dependent on sea ice porosity, and showed declining trends with increasing porosity. The sea ice flexural strength was independent on brine volume fraction, which was opposite to the phenomenon derived from cold ice. The uniaxial compressive strength showed different dependences on sea ice porosity at ductile and brittle strain rate regimes. It is clear to use three-dimensional surface to depict the variation of sea ice uniaxial compressive strength with strain rate and porosity. Furthermore, the transition strain rate from ductile to brittle behaviors of sea ice could be determined from the surface, and the transition strain rate decreased with increasing porosity. Unlike sea ice flexural strength and uniaxial compressive strength, sea ice porosity, brine volume fraction, and gas volume fraction had no statistically significant effects on sea ice strain modulus.

ACKNOWLEDGEMENTS

This research was supported by the National Natural Science Foundation of China (42 276242 and 41876219), and the Fundamental Research Funds for the Central Universit ies (DUT21RC3086).

REFERENCES

Cox, G.F.N., & Weeks, W.F., 1983. Equations for determining the gas and brine volumes in sea ice samples. *Journal of Glaciology*, 29 (102), pp.306-316.

Karulina, M., Marchenko, A., Karulin, E., Sodhi, D., Sakharov, A., & Chistyakov, P.: 2019. Full-scale flexural strength of sea ice and freshwater ice in Spitsbergen Fjords and North-West Barents Sea. *Applied Ocean Research*, 90, 101853.

Moslet, P.O., 2007. Field testing of uniaxial compression strength of columnar sea ice. *Cold Regions Science and Technology*, 48, pp.1-14.

Rantanen, M., Karpechko, A.Y., Lipponen, A., Nordling, K., Hyvärinen, O., Ruosteenoja, K., Vihma, T., & Laaksonen, A., 2022. The Arctic has warmed nearly four times faster than the globe since 1979. *Communications Earth and Environment*, 3, 168.

Schulson, E.M., 2001. Brittle failure of ice. *Engineering Fracture Mechanics*, 68, pp.1839-1887.

Timco, G.W., & Frederking, R.M.W., 1990. Compressive strength of sea ice sheets. *Cold Regions Science and Technology*, 17, pp.227-240.

Timco, G.W., & O'Brien, S., 1994. Flexural strength equation for sea ice. *Cold Regions Science and Technology*, 22, pp.285-298.

Wang, Q., Lu, P., Leppäranta, M., Cheng, B., Zhang, G., & Li, Z., 2020. Physical properties of summer sea ice in the Pacific sector of the Arctic during 2008–2018. *Journal of Geophysical Research-Oceans*, 125, e2020JC016371.

Wang, Q., Li, Z., Lu, P., Xu, Y., & Li, Z., 2022. Flexural and compressive strength of the landfast sea ice in the Prydz Bay, East Antarctic. *The Cryosphere*, 16, pp.1941-1961.